JVST B
Journal of Vacuum Science & Technology B

Ion bombardment induced formation of self-organized wafer-scale GaInP nanopillar assemblies

Cite as: J. Vac. Sci. Technol. B **38**, 012801 (2020); https://doi.org/10.1116/1.5127265
Submitted: 10 September 2019 . Accepted: 06 December 2019 . Published Online: 19 December 2019

Dennis Visser, Juliana Jaramillo-Fernandez, Gabriel Haddad, Clivia M. Sotomayor Torres, and Srinivasan Anand

COLLECTIONS

This paper was selected as Featured

View Online Export Citation CrossMark

ARTICLES YOU MAY BE INTERESTED IN

Bismuth vanadate photoanodes for water splitting deposited by radio frequency plasma reactive co-sputtering
Journal of Vacuum Science & Technology B **38**, 012203 (2020); https://doi.org/10.1116/1.5129612

High-brightness source of energetic He atoms
Journal of Vacuum Science & Technology B **38**, 012601 (2020); https://doi.org/10.1116/1.5124838

Electrical and optical properties of copper oxide thin films prepared by DC magnetron sputtering
Journal of Vacuum Science & Technology B **38**, 012803 (2020); https://doi.org/10.1116/1.5131518

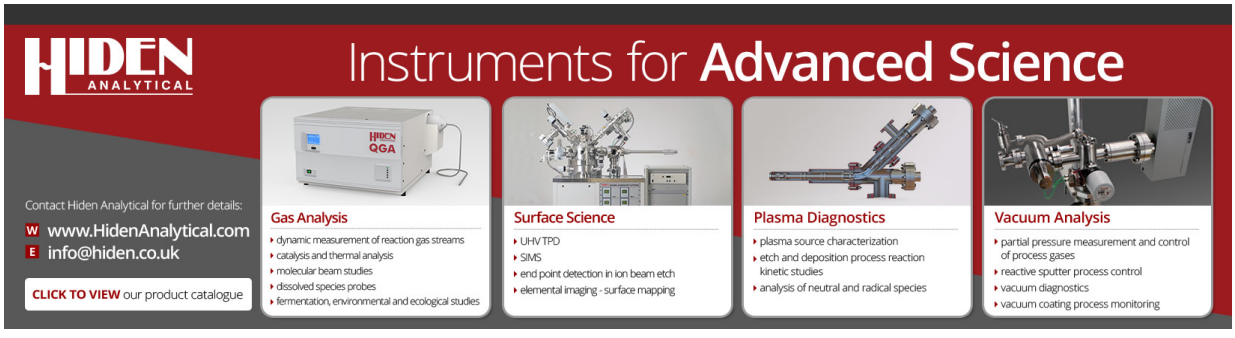

© 2019 Author(s).

JVST B
Journal of Vacuum Science & Technology B

ARTICLE

avs.scitation.org/journal/jvb

Ion bombardment induced formation of self-organized wafer-scale GaInP nanopillar assemblies

Cite as: J. Vac. Sci. Technol. B 38, 012801 (2020); doi: 10.1116/1.5127265
Submitted: 10 September 2019 · Accepted: 6 December 2019 ·
Published Online: 19 December 2019

View Online Export Citation CrossMark

Dennis Visser,[1,a] Juliana Jaramillo-Fernandez,[1] Gabriel Haddad,[1] Clivia M. Sotomayor Torres,[1,2,3] and Srinivasan Anand[1]

AFFILIATIONS

[1]Department of Applied Physics, KTH Royal Institute of Technology, Electrum 229, SE-164 40 Kista, Sweden
[2]Catalan Institute of Nanoscience and Nanotechnology (ICN2), CSIC and The Barcelona Institute of Science and Technology, Campus UAB, 08193 Bellaterra, Barcelona, Spain
[3]ICREA, Pg. Lluis Companys 23, 08010, Barcelona, Spain

[a]**Electronic mail:** dvisser@kth.se

ABSTRACT

Ion sputtering assisted formation of nanopillars is demonstrated as a wafer-scale, lithography-free fabrication method to obtain high optical quality gallium indium phosphide (GaInP) nanopillars. Compared to binary materials, little has been reported on the formation of self-organized ternary nanostructures. Epitaxial (100) $Ga_{0.51}In_{0.49}P$ layers lattice matched to GaAs were sputtered by nitrogen (N_2) ions with relatively low ion beam energies (~400 eV) to reduce ion bombardment induced damage. The influence of process parameters such as temperature, sputter duration, ion beam energy, and ion beam incidence angle on the pillar formation is investigated. The fabricated GaInP nanopillars have average diameters of ~75–100 nm, height of ~220 nm, and average density of ~$2–4 \times 10^8$ pillars/cm^2. The authors show that the ion beam incidence angle plays an important role in pillar formation and can be used to tune the pillar shape, diameter, and spatial density. Specifically, tapered to near cylindrical pillar profiles together with a reduction in their average diameters are obtained by varying the ion beam incidence angle from 0° to 20°. A tentative model for the GaInP nanopillar formation is proposed based on transmission electron microscopy and chemical mapping analysis. μ-Photoluminescence and μ-Raman measurements indicate a high optical quality of the c-GaInP nanopillars.

© 2019 Author(s). All article content, except where otherwise noted, is licensed under a Creative Commons Attribution (CC BY) license (http://creativecommons.org/licenses/by/4.0/). https://doi.org/10.1116/1.5127265

I. INTRODUCTION

Semiconductor nanopillars/wires can be used for a wide variety of applications in the fields of, e.g., optoelectronics and sensing.[1–4] They offer unique features for obtaining specific optical functions, e.g., light extraction, increased absorption, and optical nonlinearity. Nanopillar-based solar cells are of interest due to their omnidirectional broadband antireflection and light trapping abilities to achieve cheaper and more efficient solar cells.[5–8] III–V semiconductors, e.g., indium phosphide (InP) and gallium arsenide (GaAs), have the benefit of a direct bandgap, large absorption coefficients, and high conversion efficiencies. Nanostructuring of these III–V materials paves the way for implementing light manipulation functions, e.g., trapping, guiding, and antireflection.

Bottom-up[9–11] and top-down[12–14] approaches are commonly used for the fabrication of III–V nanopillars, each with their own advantages. The bottom-up approach relies mostly on a growth catalyst to initiate the nanopillar growth. To obtain dense/ordered nanopillar structures, these catalyst (e.g., gold) particles need to be patterned on the surface to enable a controlled growth of nanowires. Top-down approaches typically use surface patterning by lithography and subsequent pattern transfer into the III–V layers by etching. A number of lithography methods are commonly used, e.g., electron beam lithography, nanoimprint lithography, focused ion beam, and nanosphere lithography.[15,16] For large-scale fabrication, some important factors are the scalability of the method, cost, reduced process complexity, and process time.

© Author(s) 2019

Recently, self-organized surface nanopatterning by ion beam sputtering (IBS) at moderate (1–10 keV) and high (10–100 keV) energies has emerged.[17] The production of nanoripple[18–21] and nanodot[22–28] (periodic) nanostructures using IBS has been reported, with structure dimensions ranging from a few up to hundreds of nanometers. The advantage is that these structures can be fabricated on different materials (crystalline or amorphous) using short processing times and obtain large area coverages. Similar morphologies obtained for different materials indicate the universality of the process. A control of the fabricated nanostructures can be obtained by engineering the process parameters, e.g., ion energy, substrate temperature, ion density, and ion incidence angle.

Sigmund[29] provided the first theoretical background for understanding IBS nanostructuring, where he showed that local surface minima erode at a faster rate than local maxima leading to a surface instability; thus, the origin of the nanostructuring is based on surface-curvature-depended sputtering rates. Followed by this work, Bradley and Harper[30] reported a continuum model regarding ripple formation, and over the years, other models have been proposed taking into account the different experimental behaviors.[31–33] In 1999, Facsko *et al.*[22] reported the formation of gallium antimonite (GaSb) nanodot patterns by IBS. Since then, nanodot production has been reported in materials such as InP,[23] indium arsenide (InAs),[24] indium antimonite (InSb),[25] GaAs,[26] silicon (Si),[27] and germanium (Ge).[28] Due to this, new theoretical descriptions have been reported.[34–40] Madi *et al.*[41] and Castro *et al.*[42] changed the theoretical view and proposed a mechanism in which the sputtering pattern topographical instability is based on mass transport rather than erosion. In 2009, a self-masking process was reported by Le Roy *et al.*,[43] where an investigation of GaSb showed that one species segregates and functions as a continuously supplied etch mask. Recent works[44–46] investigated the species that should be present on the nanostructure top for binary compounds (based on sputtering yield and diffusivity), where Shipman and Bradley[44] developed a theory for ordered nanodot formation based on normal incidence ion bombardment. These works indicate that element segregation may occur after ion beam processing and that ex situ characterization may provide distorted information. Recently, the fabrication of wafer-scale InP nanopillar arrays using low energy (400 eV) IBS was reported where broadband antireflection and solar cell application were demonstrated.[8] However, compared to binary materials, little has been reported on the IBS-assisted nanopatterning of ternary structures. Examples of reported ternary structures are CdZnTe by Gago *et al.*[47] and HgCdTe by Smirnov *et al.*;[48] however, no results are reported for ternary III–V semiconductor materials. IBS pattern formation of III–V semiconductor materials is interesting due to their rapid formation rate, high aspect ratio structures due to low saturation, the occurrence of dense patterns over large surface areas, and enhanced growth rate for increasing temperatures.[43,49–51] Trynkiewicz *et al.*[52,53] discussed the mechanism of nanopillar formation in III–V semiconductor materials with special emphasis on the influence of the target temperature. However, there is still a lack of clear comprehension of the process of spontaneous ion-induced pattern formation for III–V semiconductor materials.

Here, we report on the wafer-scale, self-organized fabrication of gallium indium phosphide (GaInP) nanopillar assemblies using low energy IBS, where the main focus is on the self-organized formation of nanopillars. Although no actual application is shown in this work, direct bandgap GaInP materials are interesting for several visible range applications such as solar cells[54–56] and window layers for (GaAs-based) solar cells.[57–59] The influence of several important process parameters for the IBS process is investigated: ion beam energy, substrate temperature, processing time, and ion beam incidence angle. Scanning electron microscopy (SEM), transmission electron microscopy (TEM), energy-dispersive x-ray spectroscopy (EDS), μ-photoluminescence (PL), and μ-Raman measurements were used to characterize the fabricated GaInP nanopillars.

II. EXPERIMENT

A three grid ion beam etching system from Oxford Instruments Plasma Technology (Ionfab 300 Plus) was used to fabricate the self-organized GaInP nanopillars. A schematic of the configuration of the IBS process is shown in Fig. 1(a). The three grid ion source allows energies close to the sputtering threshold (~100 eV), which has been shown to be effective for nanopattering of GaSb.[60] Here, a directional ion beam consisting of nitrogen (N_2) ions was used to physically etch the substrate. In previous reported works, heavier ions with higher ion energies (in the keV range) were used for the formation of nanostructures by ion beam etching, leading to the degradation of the optical properties.[18–28] However, nanostructures with good crystalline cores have been reported with keV argon (Ar) ions.[22,23,51] Here, nitrogen ions with energies of only a few hundred eV were used to minimize the detrimental influence of the ion beam induced damage on the optical properties. The nitrogen beam consists of N_2^+ and N^+ species,[61] where the singly ionized process gas molecules (N_2^+) are the dominating ions (~90%); therefore, the final energy per atom is half that of the beam voltage. By using an off-normal incidence beam angle, tilted nanopillars can be fabricated [see Fig. 1(b)]. But by varying the off-normal incidence beam angle (by tilting the sample stage) while rotating the sample [see Fig. 1(c)], vertical nanopillars can be obtained where the geometry (diameter) of the nanopillars can be tuned. This work focuses on the latter configuration.

A 1 μm (100) $Ga_{0.51}In_{0.49}P$ (here on referred to as GaInP) lattice matched epitaxial layer was grown on GaAs by a metalorganic chemical vapor deposition method (obtained from ENT S.A., Warsaw, Poland). Prior to IBS experiments, a 50 nm GaAs cap layer was removed by wet etching (H_3PO_4:H_2O_2:H_2O = 3:1:25). Subsequently, the sample surface was cleaned by sonication with acetone and isopropanol, rinsed in de-ionized water, and blow dried by N_2 flow. The sample stage/platen can be heated up to 300 °C. The samples were preheated to the desired process temperature prior to sputtering. The substrate temperature is a crucial factor for the formation of nanopillars. Therefore, the influence of the processing temperature was investigated with regard to the ability to form group III-rich clusters during ion bombardment, which will function as an etch mask during sputtering. A diluted hydrogen fluoride [HF (50%)] treatment was used to remove the outer layers of the as-formed nanopillars, thereby obtaining crystalline GaInP nanopillars.

© Author(s) 2019

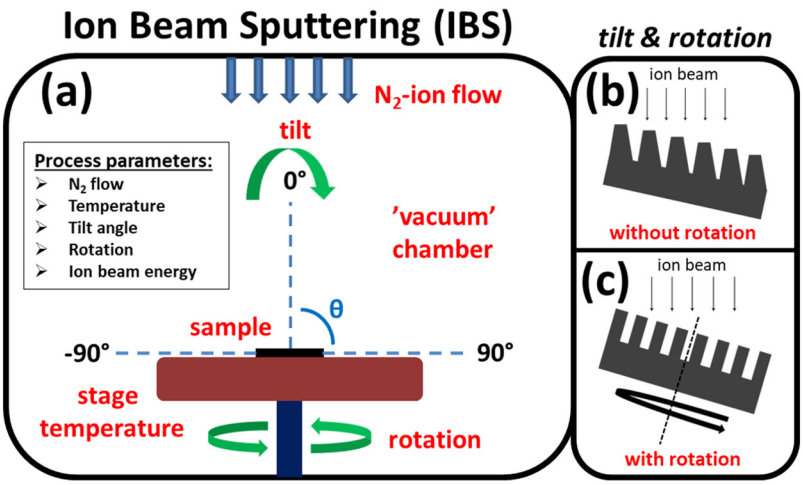

FIG. 1. (a) Schematic sketch showing the ion beam sputtering (IBS) configuration. Schematic illustration of the etch profiles obtained for a nonvertical ion beam incidence angle (b) without and (c) with sample/stage rotation.

In this work, the influence of the sample temperature (T_s: 150–270 °C), processing time (t_p: 10–40 min), ion beam voltage/energy (V_B: 200–600 V), and ion beam incidence angle (0°–20°; with rotation) has been investigated with regard to GaInP nanopillar formation. The other parameters that were not varied include the N_2 flow of 13 SCCM, beam current of 100 mA (0.6 mA/cm^2), accelerator voltage of 500 V, platen rotation speed of 20 revolutions per minute, temperature of the chiller for platen cooling of 15 °C, and pressure of the helium (He) backside cooling at 15 Torr.

III. RESULTS AND DISCUSSION

A. Configuration of the as-formed nanopillars

The formation of InP nanopillars by ion sputtering is known to arise from preferential sputtering of phosphorus (P) that makes the surface indium (In)-rich.[8] The excess In atoms diffuse and form clusters that provide self-masking. The surface diffusion of the In atoms is not only thermally driven but is also assisted by ion sputtering. In the case of GaInP also, one might expect similar mechanisms to be responsible for pillar formation. However, the diffusion and sputter yields of gallium (Ga) and In could be different. This, in turn, might also result in different elemental distribution in the formed nanopillars. Such information is also necessary for further processing (for example, to obtain crystalline nanopillars) as well as to interpret the geometrical features and optical characteristics of the nanopillars. Therefore, we first discuss the TEM and EDS results for the as-formed GaInP nanopillars. The nanopillars were fabricated using the following parameters: ion beam incidence angle of 15°, T_s of 270 °C, t_p of 10 min, and V_B of 400 V. Figure 2(a) shows a representative TEM image of the as-formed GaInP nanopillar. For TEM analysis, the pillars were scraped from the substrate using a blade and deposited on a TEM grid. Three typical regions can be distinguished along the as-formed pillar. Region I represents an In-rich top of the pillar, region II represents a Ga-rich amorphous GaInP (a-GaInP) "jacket," and region III represents a crystalline GaInP (c-GaInP) nanopillar (also indicated by the white dashed region). The supporting EDS results for regions I–III are shown in Fig. 2(b). A more detailed element analysis is included in the supplementary material (Fig. S1).[70] Figure 2(c) shows a TEM image of a c-GaInP nanopillar after removal of the Ga-rich a-GaInP shell layer and In-rich top by HF treatment. The formation of the shell layer during IBS is beneficial since this layer protects the c-GaInP core of the pillar from damage from the ion bombardment. For any device application, it is important to only use the c-GaInP nanopillar part by removing the shell layer and In-rich top. Representative high-resolution TEM images for the as-formed pillars are shown in Figs. 2(d)–2(f), where Fig. 2(d) represents the red dashed region (region I), Fig. 2(e) represents the green dashed region (region II), and Fig. 2(f) represents the blue dashed region (region III) in Fig. 2(a), respectively. Figure 2(g) shows a representative high-resolution TEM image for the c-GaInP nanopillar for the orange dashed region indicated in Fig. 2(c). A factor that should be considered related to the use of nitrogen ions is chemical modification (nitride formation). Similar nanopatterns have been produced on InP surfaces with O_2^+ ions,[62] where the formation of oxides was found to be relevant. Carlström and Anand[63] reported on the damage of InP dry etching using nitrogen sputtering, where 75 eV nitrogen milling resulted in a nitrogen penetration depth of <100 nm. It was shown that an additional annealing step can be used to remove the nitrogen content. The EDS results in Fig. 2(b) indicate nitrogen incorporation in the as-formed structures; however, nitrogen is predominantly present in the outer "jacket" layer (regions I and II).

B. Influence of sample temperature, processing time, and ion beam energy on nanopillar formation

Figure 3 shows SEM images indicating the influence of the sample temperature (T_s = 150–270 °C), processing time (t_p = 10–40 min), and ion beam energy (V_B = 200–600 V) for a 0° ion beam incidence angle. Figures 3(a)–3(c) show the influence of T_s where representative SEM images are shown for T_s taken as 190, 230, and

© Author(s) 2019

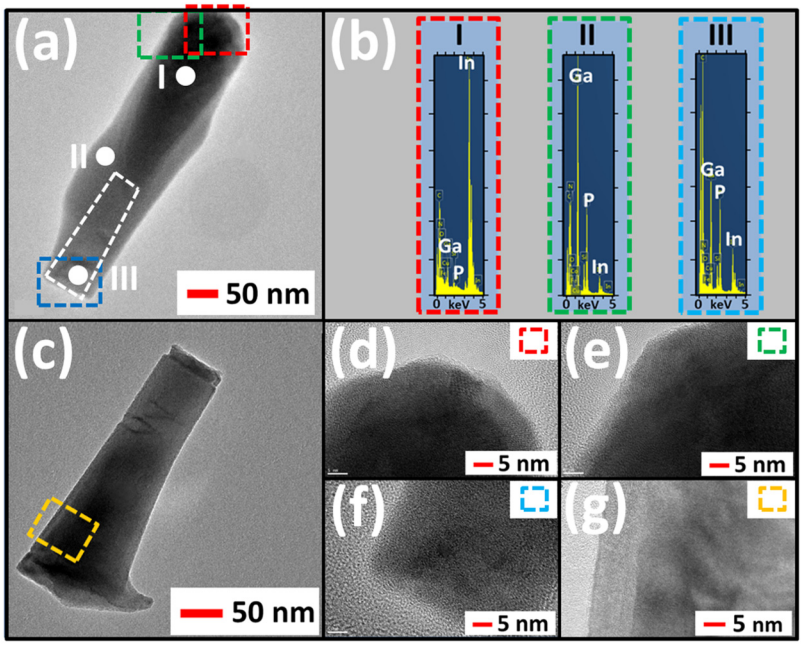

FIG. 2. Transmission electron microscopy (TEM) images of a single GaInP nanopillar for the as-formed and the resulting c-GaInP pillar fabricated with a 15° ion beam incidence angle (combined with sample rotation). (a) Shows a TEM image of the as-formed GaInP nanopillar. The white dashed region indicates the c-GaInP nanopillar. (b) Shows the energy-dispersive x-ray spectroscopy (EDS) spectra for regions I, II, and III indicated in (a). Region I shows to be In-rich, region II shows Ga-rich a-GaInP, and region III shows c-GaInP. (c) Shows a TEM image of the obtained c-GaInP nanopillar after HF treatment. (d)–(f) Shows high-resolution TEM images of the as-formed GaInP nanopillars, showing representative images for the In-rich top [red dashed region depicted in (a)], the Ga-rich a-GaInP side wall [green dashed region depicted in (a)], and the crystalline GaInP bottom part [blue dashed region depicted in (a)]. (g) Shows the crystallinity of the GaInP structure obtained after HF treatment; the representative image is related to the orange dashed region depicted in (c).

270 °C, respectively, with $t_p = 10$ min and $V_B = 400$ V. For this ion energy and sputter duration, the results show that for $T_s < 190$ °C In clusters are not formed at the surface. For $T_s = 190$ °C, In clusters are formed but only small GaInP structures are shaped underneath. When increasing T_s further to 230 °C, proper as-formed GaInP pillars are obtained, where for a higher temperature of 270 °C even longer are obtained. T_s was not further increased due to the temperature limit of the ion beam system. The results regarding T_s indicate that the height and density of the as-formed GaInP nanopillars can be tuned by controlling T_s. The optimized value of T_s is taken further on as 270 °C.

Figures 3(d)–3(f) show representative SEM images regarding the influence of t_p taken as 10, 20, and 40 min, respectively, with $T_s = 270$ °C and $V_B = 400$ V. For longer t_p, the as-formed GaInP

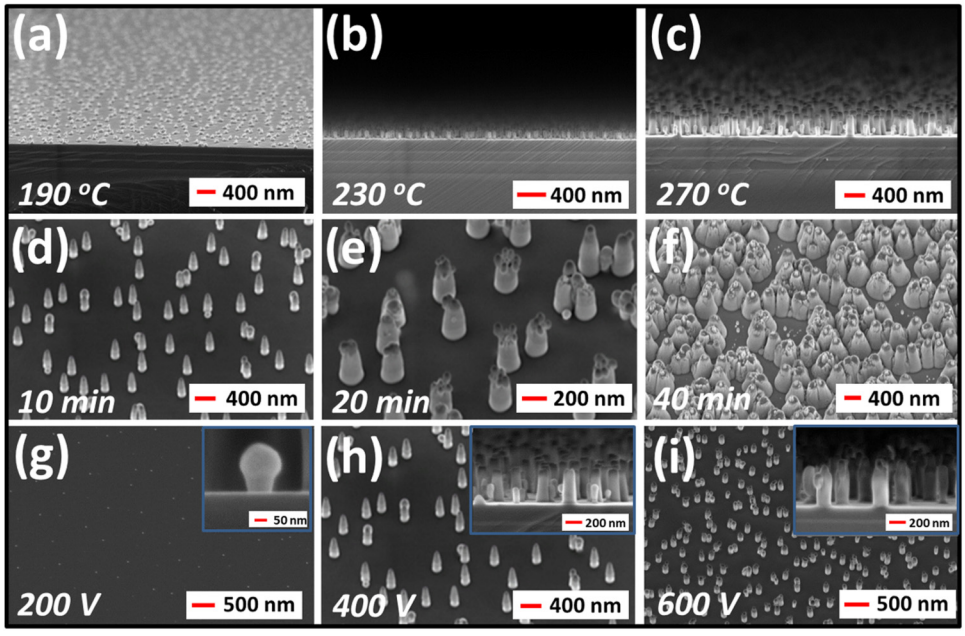

FIG. 3. Scanning electron microscopy (SEM) tilted view images showing the influence of the process parameters: (a)–(c) temperature (190–270 °C), (d)–(f) processing time (10–40 min), and (g)–(i) ion beam voltage (200–600 V). The insets in (g)–(i) show the respective cross sections of the as-formed nanostructures.

© Author(s) 2019

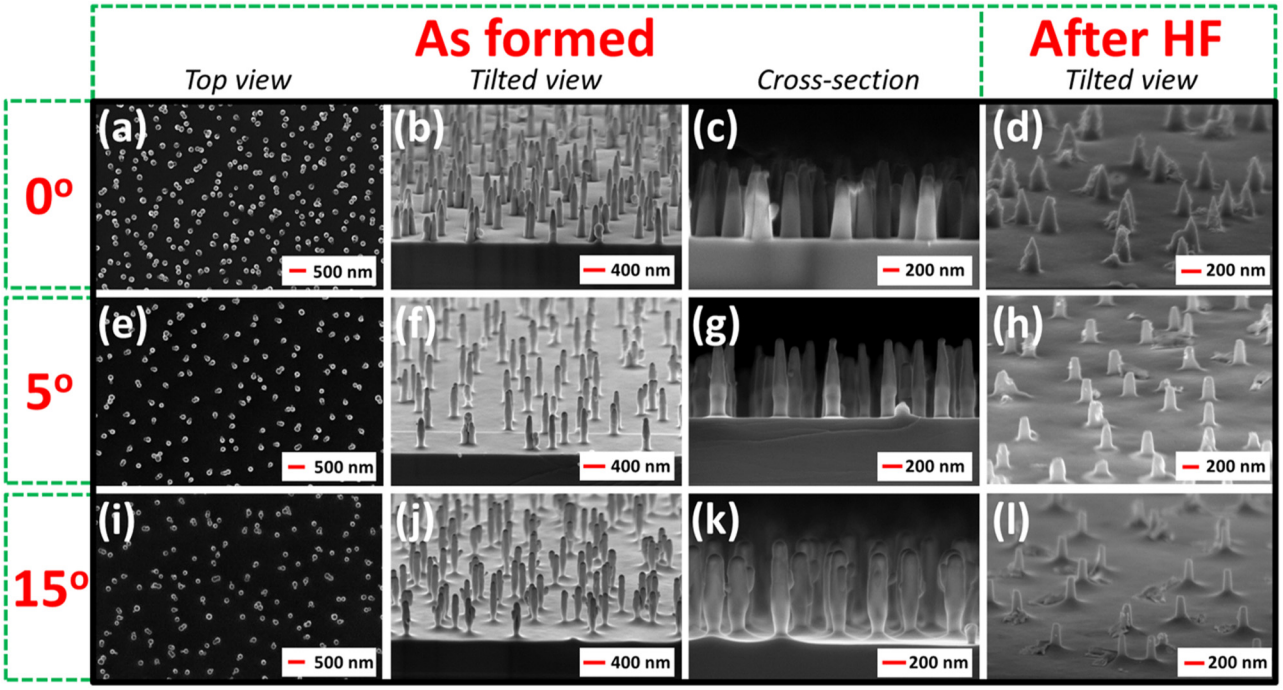

FIG. 4. Scanning electron microscopy (SEM) images of the obtained GaInP nanopillars (as-formed and after HF treatment) for an ion beam incidence angle of (a)–(d) 0°, (e)–(h) 5°, and (i)–(l) 15°, where the top view [(a), (e), and (i)], tilted view [(b), (f), and (j)], and cross section [(c), (g), and (k)] are shown for the as-formed GaInP nanopillar assemblies. Additionally, tilted view images [(d), (h), and (l)] of the c-GaInP nanopillar assemblies (obtained after HF treatment) are shown.

pillars become longer in height. Additionally, the density of the as-formed pillars increases due to the formation of new In clusters between the original clusters (for shorter t_p) and the apparent broadening of the as-formed pillar diameter, where the broadening of the "jacket" of the pillar is most likely due to the diffusion of Ga (and In) atoms to the side walls and redeposition of P. The value for t_p is further on taken as 10 min.

Figures 3(g)–3(i) show representative SEM images for the influence of V_B taken as 200, 400, and 600 V, respectively, with $T_s = 270°$ and $t_p = 10$ min. For $V_B = 200$ V, relatively low density In cluster sites are formed, where barely a shape is formed below the In mask [see Fig. 3(g)]. For $V_B = 400$ V, pillar shapes are formed, and $V_B = 600$ V results in even taller as-formed pillars and slightly higher pillar density. Although larger and higher density as-formed nanopillars are obtained for $V_B = 600$ V, it is best to limit the ion beam energy bombardment to prevent degrading of optical properties. Due to this, the optimal value for V_B is taken as 400 V.

C. Influence of the ion beam incidence angle on the geometry and spatial arrangement of the (c-GaInP) nanopillars

The influence of the ion beam incidence angle has been investigated for angles varying between 0° and 20°, with a step size of 5°. For this, the previously mentioned process parameters were used. Figure 4 shows representative SEM images for three of those angles (0°, 5°, and 15°); where for the as-formed pillars top view, tilted view and cross section images are included and for the resulting c-GaInP nanopillars (obtained after HF treatment) only tilted view images. For some of the as-formed pillars, a protrusion was observed on the side wall of the pillars. EDS analysis of this protrusion indicates that this consists of Ga-rich a-GaInP; representative data for this are included in the supplementary material (Fig. S2).[70] However, this protrusion is removed during the HF treatment, and therefore, no further investigations were done regarding its occurrence. The resulting pillar ensembles show that the ion beam incidence angle influences the density and shape of the obtained GaInP nanopillars (before and after HF treatment). Figure 5 summarizes the results regarding the influence on the nanopillar height, average density, and diameter due to the ion beam incidence angle based on SEM images analysis. As can be seen in Fig. 5(a), the height of the as-formed pillars changes with the applied incidence angle, varying between ~550 and 800 nm. However, the height of the obtained c-GaInP (after HF treatment) shows to be similar for all investigated incidence angles and results in a height of ~220 nm. As can be seen in Fig. 5(b), the average density also fluctuates with regard to the incidence angle, varying between ~2 and 4×10^8 pillars/cm^2. An interesting observation for the as-formed nanopillars is that the incidence angle dependence of the height of the pillars is inversely related to the density, where pillars with a larger height

© Author(s) 2019

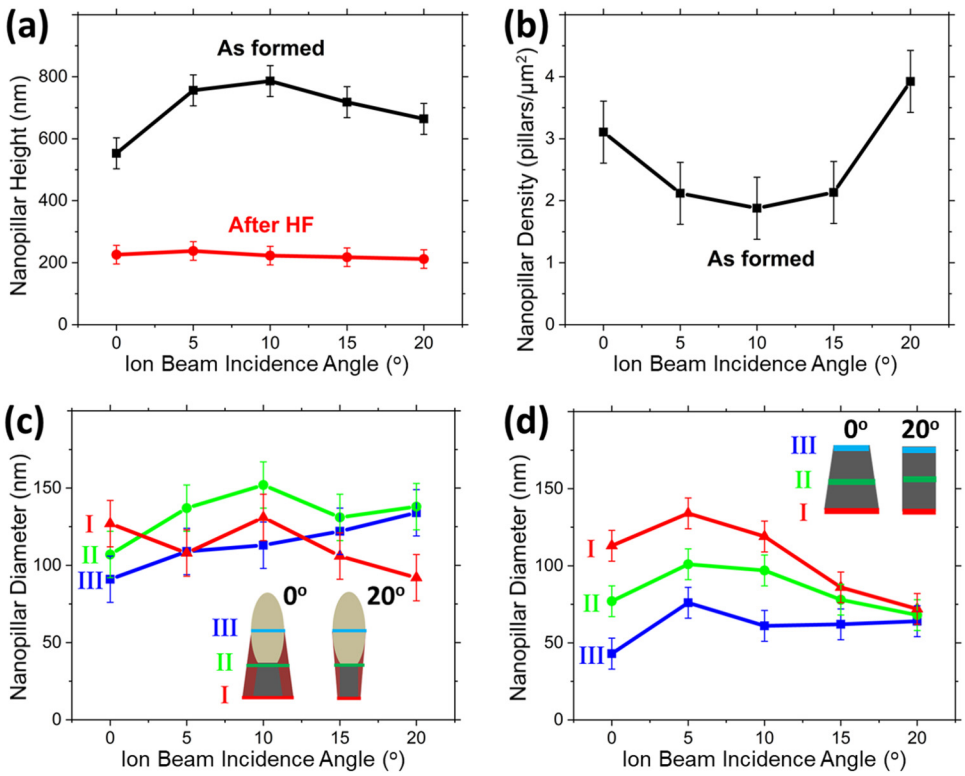

FIG. 5. Graphs showing the influence of the ion beam incidence angle (angles of 0°–20°) on the GaInP nanopillar (a) height, (b) average density, and the pillar diameter of the (c) as-formed and (d) c-GaInP nanopillars (after HF treatment), respectively. In (c) and (d), the nanopillar diameters were measured as indicated in the insets of both figures.

show a lower density. Figures 5(c) and 5(d) show the diameter dependence for the as-formed and c-GaInP nanopillars with regard to the incidence angle. This has been done at three height positions of the pillar to indicate the pillar shape: bottom (I), middle (II), and top (III) of the pillar [see for further clarification the inset in Figs. 5(c) and 5(d)]. The diameter of the as-formed pillars varies between ~90 and 150 nm, where the top and middle diameters increase for increasing incidence angle and the bottom diameter decreases. The average diameter of the c-GaInP nanopillars is ~75–100 nm and changes with the ion beam incidence angle. The shape of the pillar changes from a pillar to a wire shape when increasing the incidence angle from 0° to 20°.

D. Tentative model for nanopillar formation

Figure 6 shows a tentative model that is based on TEM, EDS, and SEM results in combination with measured chemical mapping plots that are included in the supplementary material (Figs. S3 and S4).[70] The formation of the GaInP nanopillars is due to the preferential sputtering of P compared to Ga and In, where Ga is preferentially sputtered compared to In. The In is partially sputtered away but additionally excess In forms at the surface leading to In enrichment. Diffusion of this excess In takes place and results in In-rich clusters on the surface within its diffusion length, eventually acting as an etch mask. The diffusion of the excess atoms is related to the processing temperature and increases when the temperature increases. The continuous ion bombardment additionally contributes to providing extra energy to the migrating In atoms and is generally seen as lowering of the energy barrier for diffusion. Newly formed In atoms preferably diffuse to already formed In clusters within its diffusion length and thereby sustain the etch mask during sputtering as the surface topography evolves. This process is continuous until the length of the formed pillars is longer than the diffusion length of the In atoms, resulting in that the sputtering of the In mask/clusters dominates due to the lack of additional In atoms provided to the In mask. When the length of the nanopillars reaches within the diffusion length, additional In atoms can reach the top of the pillars and again form the etch mask. This results in that a maximum nanopillar length can be obtained, which is related to the diffusion length of the In atoms. Furthermore, a shadowing effect should be taken into account for off-normal ion beam incidence angles. In addition to In, Ga atoms also diffuse along the surface. However, their diffusion properties could be different. The obtained results indicate that the Ga atoms play a minor role in the formation of the top etch mask but accumulate at the sides of the as-formed pillars, where redeposition of the sputtered P atoms also occurs. The dynamics of the surface conditions and evolution during IBS of GaInP is a complex process involving three species of atoms, modification of the surface morphology, changes of the chemical composition, and surface diffusion of atoms influenced by thermal/ion-assisted factors. A number of

© Author(s) 2019

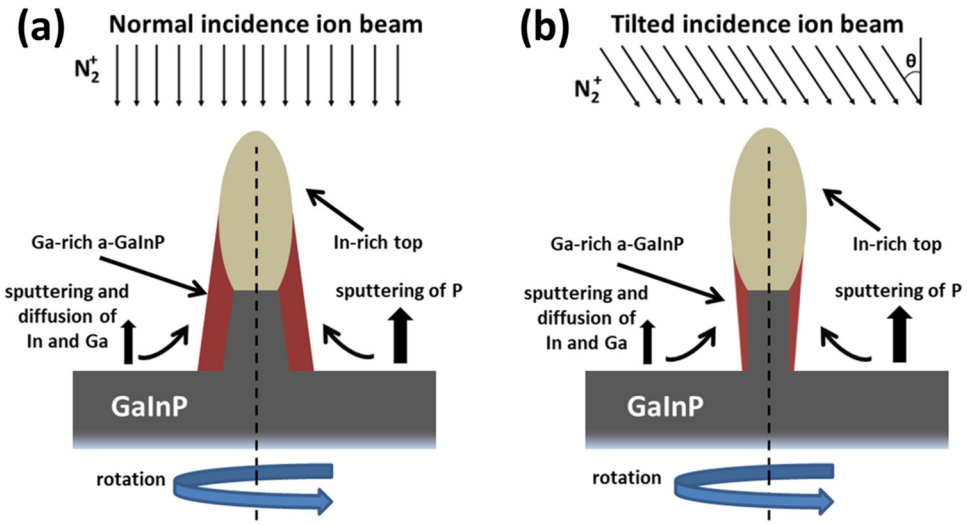

FIG. 6. Tentative model for the as-formed fabricated GaInP nanopillars at (a) normal (0°) and (b) tilted (20°) ion beam incidence angles (with sample/stage rotation). In the model, the In-rich and Ga-rich amorphous GaInP (a-GaInP) regions are indicated with an arrow. The gray color of the structure indicates the crystalline GaInP (c-GaInP).

process parameters influence the GaInP nanopillar formation, e.g., ion species, ion energy (V_B), T_s, and ion beam incidence angle. A detailed description of the mechanism of the GaInP nanopillar formation with regard to the geometry, spatial density, elemental distribution, and material quality is beyond the scope of this work and requires an extensive study of the role of various parameters involved. In this work, preliminary investigations were done for some of these process parameters.

E. Photoluminescence and Raman characterization

μ-PL and μ-Raman measurements were performed (source wavelength of 514 nm) to characterize the optical properties of the fabricated GaInP nanopillars (see Fig. 7). The laser power and the spot size were ~8 μW and ~30 μm, respectively, for μ-PL and ~3.6 mW and ~2 μm for μ-Raman, respectively. μ-Raman measurements were done on the as-formed as well as on the c-GaInP nanopillars and μ-PL measurements only on the c-GaInP nanopillars.

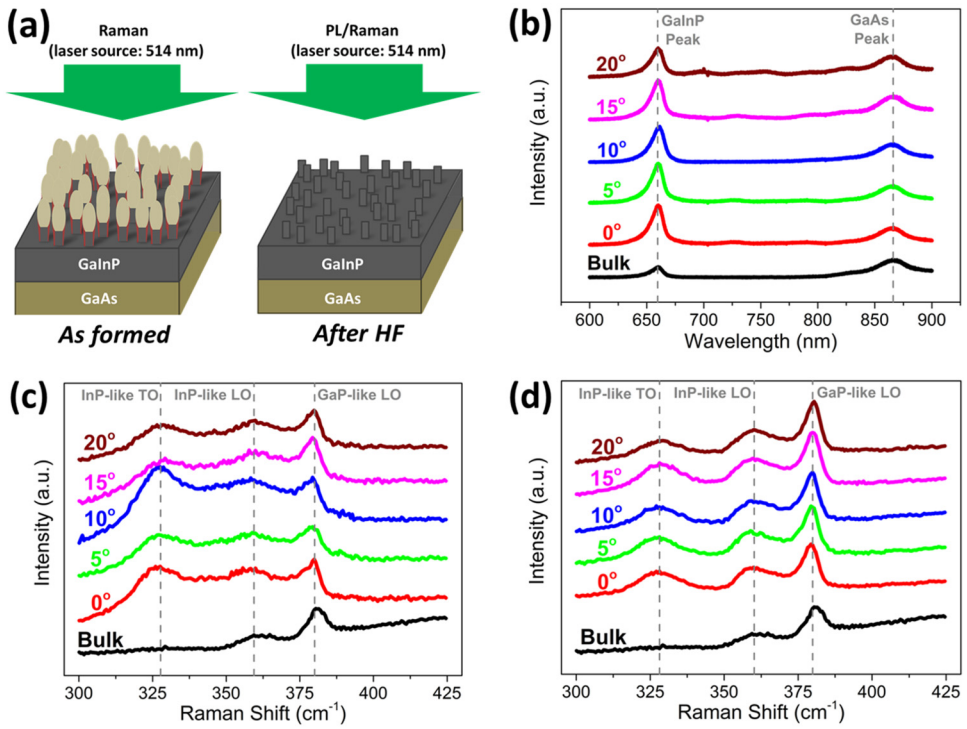

FIG. 7. Measured μ-PL and μ-Raman characteristics for the GaInP nanopillars fabricated at ion beam incidence angles varying between 0° and 20° for the cases: as-formed and c-GaInP (after HF treatment) nanopillar assemblies. (a) Shows schematics for the measured structures both for μ-PL and μ-Raman measurements, where a laser source at 514 nm was used. (b) Shows the μ-PL results for the c-GaInP nanopillars. (c) Shows the μ-Raman characteristics for the as-formed and (d) for the c-GaInP nanopillar assemblies.

© Author(s) 2019

The as-formed pillars are covered by metallic and amorphous layers and, hence, not investigated by PL. Figure 7(b) shows that the μ-PL results where both the peaks related to GaInP (at ~657 nm) and GaAs (at ~870 nm) are indicated with a vertical dashed line. Data are included for "bulk" GaInP with a layer thickness of ~600 nm. The μ-PL spectra show similar results for almost all incidence angles. For the incidence angle of 0°, a higher peak is observed for both GaInP and GaAs peaks, though the direct comparison of PL intensities is often difficult due to the fact that it is a local and spacially dependent measurement; yet an increase in peak value might suggest higher light extraction. Figures 7(c) and 7(d) show the μ-Raman measurement results for the as-formed and the c-GaInP nanopillar assemblies, respectively. For the as-formed pillars, an increase in the background signal can be observed due to the presence of the metal (In/Ga) shell [see Fig. 7(c)]. This signal is generally ascribed to the scattering of electron–hole pairs in the surface of the metal shell by Raman active modes.[64–69] Such background signal is not present for the c-GaInP case [see Fig. 7(d)], where the metal shell is removed. The spectra are shown relative to "bulk" GaInP. The structures exhibit an InP-like longitudinal optical (LO) mode at ~360 cm^{-1} and a GaP-like LO at ~380 cm^{-1}. The transverse optical mode peak at ~330 cm^{-1} is not visible for the "bulk" structure, since it is symmetry-forbidden for the (100) surface, though this peak is prominent for the self-organized GaInP nanopillar structures for all the investigated ion beam incidence angles due to symmetry breaking of the crystal at the surface.

IV. SUMMARY AND CONCLUSIONS

Wafer-scale, self-organized GaInP nanopillars were obtained based on an IBS process using low energy (~400 eV) nitrogen (N_2) ions. In comparison to binary materials, little has been reported on the self-organized formation of ternary materials by IBS. High optical quality crystalline GaInP (c-GaInP) nanopillar assemblies were obtained with an average pillar diameter of ~75–100 nm, height of ~220 nm, and average density of ~2–4 × 10^8 pillars/cm^2. Initial investigations regarding process parameters such as sample temperature, processing time (fluence), ion beam energy, and ion beam incidence angle were performed to show their influence on the formation, geometry, and density of the pillars. Temperatures between 150 and 270 °C were investigated, and the results indicate that a temperature of >190 °C is required for obtaining pillar formation. By increasing the temperature further, the geometry (height) and the density of the as-formed pillars increase. Longer processing times resulted not only in higher pillars but additionally increased the density of the pillars. The ion beam energy [i.e., beam voltage (V_B)] should be limited to prevent degradation of the optical properties of the fabricated structures; this was confirmed by μ-PL and μ-Raman characterization. Beam voltages between 200 and 600 V were investigated, and it was observed that a V_B of 400 V is sufficient for obtaining nanopillar structures. Finally, the influence of the ion beam incidence angle indicates that the average diameter can be tuned and that additionally the geometry of the nanostructures can be changed from a pillar to a wire shape, where the density of the pillars/wires also changes with the incidence angle. A tentative model was proposed based on results from TEM, EDS, and chemical mapping plots.

ACKNOWLEDGMENTS

The authors would like to acknowledge the support from the Linné Center for Advanced Optics and Photonics (ADOPT; Grant No. 349-2007-8664), the Swedish Research Council (VR), and the Swedish Energy Agency (Energimynigheten; Grant Nos. 45199-1 and 42028-1). The authors thank Frederik Gustavsson for the TEM and EDS measurements.

REFERENCES

[1]H. J. Joyce *et al.*, Prog. Quantum Electron. **35**, 23 (2011).
[2]Y. Zhang, J. Wu, M. Aagesen, and H. Liu, J. Phys. D: Appl. Phys. **48**, 1 (2015).
[3]V. Kugel and H.-F. Ji, J. Nanosci. Nanotechnol. **14**, 6469 (2014).
[4]D. Visser, B. D. Choudhury, I. Krasovska, and S. Anand, Opt. Express **25**, 12171 (2017).
[5]Z. Fan, D. J. Ruebusch, A. A. Rathore, R. Kapadia, O. Ergen, P. W. Leu, and A. Javey, Nano Res. **2**, 829 (2009).
[6]D. Liang, Y. Kang, Y. Huo, Y. Chen, Y. Cui, and J. S. Harris, Nano Lett. **13**, 4850 (2013).
[7]C. Battaglia, J. Xu, M. Zheng, X. Yin, M. Hettick, K. Chen, N. Haegel, and A. Javey, Adv. Energy Mater. **4**, 1400061 (2014).
[8]R. Sanatinia, A. Berrier, V. Dhaka, A. P. Perros, T. Huhtio, H. Lipsanen, and S. Anand, Nanotechnology **26**, 415304 (2015).
[9]K. Tomioka, J. Mater. Res. **26**, 2127 (2011).
[10]R. R. Lapiere *et al.*, Phys. Status Solidi RRL **7**, 815 (2013).
[11]V. Dagyte, "Growth and optical properties of III-V semiconductor nanowires: Studies relevant for solar cells," Ph.D. thesis (Lund University, 2018).
[12]H. Wang, M. Sun, K. Ding, M. T. Hill, and C.-Z. Ning, Nano Lett. **11**, 1646 (2011).
[13]S. Naureen, R. Sanatinia, N. Shahid, and S. Anand, Nano Lett. **11**, 4805 (2011).
[14]S. Naureen, N. Shahid, R. Sanatinia, and S. Anand, Adv. Funct. Mater. **23**, 1620 (2013).
[15]A. Pimpin and W. Srituravanich, Eng. J. **16**, 37 (2011).
[16]P. Colson, C. Henrist, and R. Cloots, J. Nanomater. **2013**, 948510 (2013).
[17]Z. Wang, "Towards functional nanomaterials," *Lecture Notes in Nanoscale Science and Technology*, (Springer, Dordrecht, 2009), Vol. 5(5), p. 323.
[18]A. Karen, A. Okuno, F. Soeda, and I. Ishitani, J. Vac. Sci. Technol. A **9**, 2247 (1991).
[19]S. W. Maclaren, J. E. Baker, W. L. Finnegan, and C. M. Loxton, J. Vac. Sci. Technol. A **10**, 468 (1992).
[20]C. V. Demanet, J. B. Malherbe, N. G. van der Berg, and V. Sankar, Surf. Interface Anal. **23**, 433 (1995).
[21]D. Datta, S. R. Bhattacharyya, T. K. Chini, and M. K. Sanyal, Nucl. Instrum. Meth. B **193**, 596 (2002).
[22]S. Facsko, T. Dekorsy, C. Koerdt, C. Trappe, H. Kurz, A. Vogt, and H. L. Hartnagel, Science **285**, 1551 (1999).
[23]F. Frost, A. Schindler, and F. Bigl, Phys. Rev. Lett. **85**, 4116 (2000).
[24]F. Frost, B. Ziberi, T. Höche, and B. Rauschenbach, Nucl. Instrum. Meth. B **216**, 9 (2004).
[25]S. Facsko, H. Kurz, and T. Dekorsy, Phys. Rev. B **63**, 165329 (2001).
[26]T. Kumar, M. Kumar, G. Gupta, R. K. Pandey, S. Verma, and D. Kanjilal, Nanoscale Res. Lett. **7**, 1 (2012).
[27]J. Muñoz-García, L. Vásquez, M. Castro, R. Gago, A. Redondo-Cubero, A. Moreno-Barrado, and R. Cuerno, Mat. Sci. Eng. R **86**, 1 (2014).
[28]B. Ziberi, F. Frost, and B. Rauschenbach, Surf. Sci. **600**, 3757 (2006).
[29]P. Sigmund, Phys. Rev. **184**, 383 (1969).
[30]R. M. Bradley and J. M. E. Harper, J. Vac. Sci. Technol. A **6**, 2390 (1988).
[31]R. Cuerno and A. L. Barabási, Phys. Rev. Lett. **74**, 4746 (1995).
[32]M. A. Makeev and A. L. Barabási, Appl. Phys. Lett. **71**, 2800 (1997).
[33]M. Paniconi and K. R. Elder, Phys. Rev. E **56**, 2713 (1997).
[34]B. Kahn, H. Jeong, and A. L. Barábasi, Appl. Phys. Lett. **78**, 805 (2001).

© Author(s) 2019

[35]M. A. Makeev, R. Cuerno, and A. L. Barábasi, Nucl. Instrum. Meth. B **97**, 185 (2002).
[36]U. Valbusa, C. Boragno, and F. Buatier de Mongeo, J. Phys. Condens. Matter **14**, 8153 (2002).
[37]S. Facsko, T. Bobek, A. Stahl, H. Kurz, and T. Dekorsy, Phys. Rev. B **69**, 153412 (2004).
[38]M. Castro, R. Cuerno, L. Vázquez, and R. Gago, Phys. Rev. Lett. **94**, 016102 (2005).
[39]H. H. Chen, O. A. Orquidez, S. Ichim, L. H. Rodriguez, M. P. Brenner, and M. J. Aziz, Science **310**, 294 (2005).
[40]J. Muñoz-García, M. Castro, and R. Cuerno, Phys. Rev. Lett. **96**, 086101 (2006).
[41]C. S. Madi, E. Anzenberg, K. F. Ludwig, Jr., and M. J. Aziz, Phys. Rev. Lett. **106**, 066101 (2011).
[42]M. Castro, R. Gago, L. Vázquez, J. Muñoz-García, and R. Cuerno, Phys. Rev. B **86**, 214107 (2012).
[43]S. Le Roy, E. Barthel, N. Brun, A. Lelarge, and E. Søndergård, J. Appl. Phys. **106**, 094308 (2009).
[44]P. D. Shipman and R. M. Bradley, Phys. Rev. B **84**, 085420 (2011).
[45]O. El-Atwani, J. P. Allain, A. Cimaroli, A. Suslova, and S. Ortoleva, J. Appl. Phys. **110**, 074301 (2011).
[46]C. Palacio, J. Olvera, J. L. Plaza, and E. Diéguez, Surf. Coat. Technol. **206**, 3146 (2012).
[47]R. Gago, L. Vázaquez, F. J. Palomares, F. Agulló-Rueda, M. Vinnichenko, V. Carcelén, J. Olvera, J. L. Plaza, and E. Diéguez, J. Phys. D Appl. Phys. **46**, 455302 (2013).
[48]A. B. Smirnov, R. K. Savkina, R. S. Udovytska, O. I. Gudymenko, V. P. Kladko, and A. A. Korchovyi, Nanoscale Res. Lett. **12**, 320 (2017).
[49]I. S. Nerbø, M. Kildemo, S. Le Roy, I. Simonsen, E. Søndergård, L. Holt, and J. C. Walmsley, Appl. Opt. **47**, 5130 (2008).
[50]Y. Yuba, S. Hazama, and K. Garno, Nucl. Instrum. Methods Phys. Res. B **206**, 648 (2003).
[51]S. K. Mohanta and R. K. Soni, Appl. Phys. Lett. **88**, 043101 (2006).
[52]E. Trynkiewicz, B. R. Jany, A. Janas, and F. Krok, J. Phys. Condens. Matter **30**, 304005 (2018).
[53]E. Trynkiewicz, B. R. Jany, D. Wrana, and F. Krok, Appl. Surf. Sci. **427**, 349 (2018).
[54]D. Shahrjerdi *et al.*, Appl. Phys. Lett. **100**, 053901 (2012).
[55]X. Li, T. Shi, G. Liu, L. Wen, B. Zhou, and Y. Wang, Opt. Express **23**, 25316 (2015).
[56]Y. Wang, R. Zhang, Z. Zhang, B. Qiu, S. Wang, and X. Wu, Sol. Energy Mater. Sol. Cells **169**, 33 (2017).
[57]J. Plá, M. Barrera, and F. Rubinelli, Semicond. Sci. Technol. **22**, 1122 (2007).
[58]R. Y. Zhang, B. Shao, J. R. Dong, K. Huang, Y. M. Zhao, S. Z. Yu, and H. Yang, Opt. Mater. Express **2**, 173 (2012).
[59]K. J. Schmieder *et al.*, "GaInP window layers for GaAsP on SiGe/Si single and dual-junction solar cells," in 2013 IEEE 39th Photovoltaic Specialists Conference (PVSC), Tampa, FL, 2013, pp. 2462–2465.
[60]O. El-Atwani, S. Gonderman, and J. P. Allain, J. Appl. Phys. **114**, 104308 (2013).
[61]M. Zeuner and Jürgen Meichsner, J. Appl. Phys. **80**, 611 (1996).
[62]S. K. Tan, R. Liu, C. H. Sow, and A. T. S. Wee, Nucl. Instrum. Methods Phys. Res. B **248**, 83 (2006).
[63]C. F. Carlström and S. Anand, J. Vac. Sci. Technol. B **19**, 1905 (2001).
[64]E. Burnstein, Y. J. Chen, C. Y. Chen, S. Lundquist, and E. Tosatti, Solid State Commun. **29**, 567 (1979).
[65]A. Otto, J. Timper, J. Billmann, G. Kovacs, and I. Pockrand, Surf. Sci. **92**, L55 (1980).
[66]T. E. Furtak and J. Reyes, Surf. Sci. **93**, 351 (1980).
[67]R. Monreal, F. Flores, Y. Gao, and T. López-Ríos, Europhys. Lett. **4**, 115 (1987).
[68]B. J. Murdoch, A. J. Barlow, I. W. Fletcher, and P. J. Cumpson, Appl. Phys. Lett. **111**, 081603 (2017).
[69]A. J. Barlow, N. Sano, B. J. Murdoch, J. F. Portoles, P. J. Pigram, and P. J. Cumpson, Appl. Surf. Sci. **459**, 678 (2018).
[70]See supplementary material at https://doi.org/10.1116/1.5127265 for more data regarding the detailed energy-dispersive X-ray spectroscopy (EDS) results for the as formed GaInP nanopillars (Fig. S1), EDS results for an observed protrusion on the side of some of the as formed nanopillars (Fig. S2), chemical mapping plots for the as formed pillars (Fig. S3), and scanning electron microscopy (SEM) images for the as formed and after HF obtained nanopillars—including the ion beam incidence angles of 10° and 20° (Fig. S4).

© Author(s) 2019